

# An Image-Based Approach for Preisach Function Calculation

Hisashi Endo, Seiji Hayano, and Yoshifuru Saito, *Member, IEEE*

**Abstract**—This paper proposes an image-based calculation of Preisach function. The function is calculated from a series of distinct magnetized domain images. The domain images derive the state transition matrices from the image Helmholtz equation, which is a governing partial differential equation of digital dynamic images. It is described that the state transition matrix of the equation makes it possible to approximate the Preisach function. An intensive verification is carried out using scanning electron microscope domain images of a grain-oriented electrical steel. The magnetization curve reconstructed by means of the state transition matrices is shown to closely reproduce experimental result. Moreover, the state transition matrices reveal the iron loss generating parts on the target specimen.

**Index Terms**—Digital dynamic image analysis, image Helmholtz equation, Preisach function.

## I. INTRODUCTION

MAGNETIZATION modeling such as Preisach and Chua type models is essential to take hysteresis and/or saturation properties into account for magnetic field calculation based on differential equations [1]–[4]. Since it is difficult to measure the flux density  $B$  as well as field  $H$  due to the demagnetization of magnetic thin films, investigation on microscopy-based measurement such as Kerr effect has been spurred [5]. The magnetized states can be visualized as contrast of the images by available domain observation techniques [6]. This background inspires this study to derive the Preisach function  $\Psi$  from a finite number of distinct magnetic domain images.

In order to derive the Preisach function from domain images, the present paper employs the image Helmholtz equation [7], which is a governing differential equation of the digital dynamic images. The state transition matrix of the equation equivalently represents the characteristic values of the physical dynamic system visualized by finite number of images. In case of a series of distinct domain images, the physical meanings of elements constituting the state transition matrix are obtained by relating them to the Preisach functions. Moreover, the magnetization curve is generated as solutions of the image Helmholtz equation.

A series of scanning electron microscope (SEM) domain images of a grain-oriented electrical steel instead of a magnetic thin film has been studied in this paper to compare with conventional magnetization curve measurement.

## II. IMAGE-BASED PREISACH FUNCTION CALCULATION

### A. Key Idea

To derive the Preisach function from given domain images, an analytical solution with the Preisach function is considered. In [4] and [8], relationship between the flux density  $B$  and field  $H$  has been clarified by a constitutive equation

$$H = H_e + H_c = \frac{1}{\mu}B + \frac{1}{\Psi} \frac{dB}{dH} \quad (1)$$

where  $H_e$  and  $H_c$  are applied and coercive fields, respectively, and  $\mu$  is permeability. In addition, their intensive numerical and experimental works have verified the validity of (1). According to [8], an analytical solution of (1) assuming the constant  $\mu$  and  $\Psi$  gives

$$\begin{aligned} B &= \mu H + [B_0 - \mu H] \exp\left(-\frac{\Psi}{\mu} H\right) \\ &= B_f + [B_0 - B_f] \exp(-\lambda H) \end{aligned} \quad (2)$$

where  $B_f$  and  $B_0$  are the final and initial flux densities, respectively, and  $\lambda$  is characteristic value. When we have the three magnetic flux densities  $B_i$ ,  $B_{i+1}$ , and  $B_{i+2}$  as the domain images during the field change  $\Delta H_i$ , (2) can be rewritten by

$$B_{i+1} = B_{i+2} + [B_i - B_{i+2}] \exp(-\lambda \Delta H_i). \quad (3)$$

Hence, modifying (3) gives the Preisach function

$$\Psi = \mu \lambda = \frac{\mu}{\Delta H_i} \ln \left[ \frac{B_{i+1} - B_{i+2}}{B_i - B_{i+2}} \right]. \quad (4)$$

Equation (4) is the principal idea of our method.

### B. Experiment of Domain Image Observation

In this method,  $B_i$ ,  $B_{i+1}$ , and  $B_{i+2}$  in (3) and (4) are assumed to be the averaged contrasts of magnetized domain images. Fig. 1 shows the SEM domain images of a grain-oriented electrical steel under the distinct magnetized states [6]. The specimen is the ORIENTCORE·HI-B (Nippon Steel Corporation product) without surface coating and its thickness is 0.23 mm. The backscattered electron observation is carried out at 160 keV acceleration. In this condition, the domain patterns 10  $\mu\text{m}$  depth from the surface could be visualized as shown in Fig. 1 [9]. The external field is applied to rolling direction with sloping excitation. The conditions of domain images used in this paper are listed in Table I.

Manuscript received February 14, 2002; revised May 28, 2002.

The authors are with the Graduate School of Engineering, Hosei University, Tokyo 184-8584, Japan. (e-mail: endo@ysaitoh.k.hosei.ac.jp).

Digital Object Identifier 10.1109/TMAG.2002.803615.

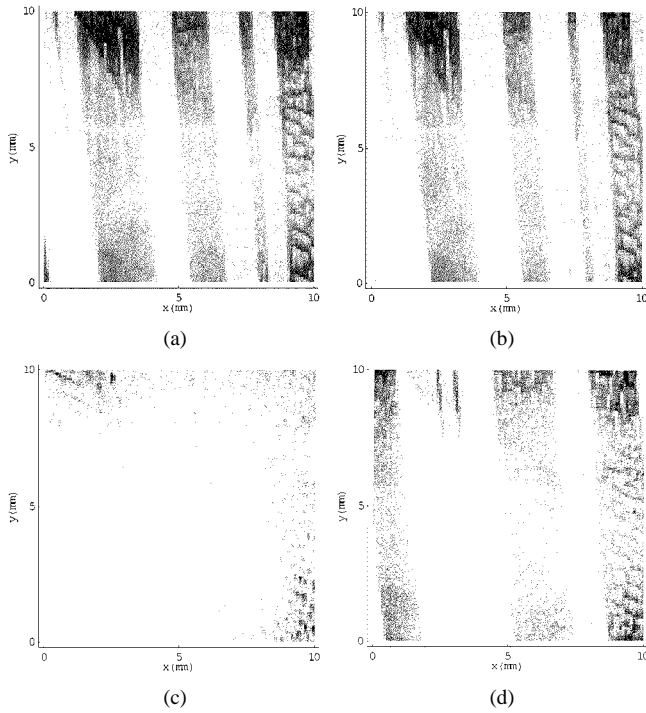


Fig. 1. Magnetic domain images of a grain-oriented electrical steel observed by SEM ( $100 \times 100$  pixels,  $0.1$  mm/pixel). (a)–(d) are the domain images numbered as 1, 2, 10, and 19 in Table I, respectively.  $y$  direction is the rolling direction and applied field axis.

TABLE I  
CONDITIONS OF MEASURED DOMAIN IMAGES  $H$ : EXTERNAL MAGNETIC FIELD INTENSITY,  $B$ : FLUX DENSITY

Image No.	$H$ (A/m)	$B$ (T)	Image No.	$H$ (A/m)	$B$ (T)
1	0.00	0.00	13	214.13	1.93
2	2.85	0.10	14	160.37	1.92
3	9.26	1.63	15	98.68	1.91
4	24.16	1.73	16	54.66	1.84
5	30.23	1.78	17	28.53	1.83
6	54.59	1.84	18	3.73	1.77
7	84.92	1.86	19	0.00	1.73
8	115.39	1.88	20	-4.60	1.73
9	160.69	1.90	21	-5.95	-0.06
10	236.32	1.92	22	-7.45	-1.43
11	324.31	1.95	23	-9.07	-1.56
12	269.64	1.95	24	-11.50	-1.62

### C. Image Helmholtz Equation

To analyze the dynamic images, we have proposed a Helmholtz-type equation [7]. Suppose that a domain image is composed of a two-dimensional scalar field  $U$ , and then the dynamics of domains can be represented by the image Helmholtz equation. In magnetized state, the domain motion is caused by field  $H$ ; therefore, the image Helmholtz equation takes into account a derivative term of the field  $H$ , thus

$$\nabla^2 U + \varepsilon \frac{\partial U}{\partial H} = -\sigma \quad (5)$$

where  $\varepsilon$  and  $\sigma$ , respectively, denote a domain motion parameter and an image source density given by the Laplacian of final image  $U_{\text{Final}}$  [10]. The first and second terms on the left in (5)

express the spatial expanse and transition of image to the variable  $H$ , respectively. In (5), the parameter  $\varepsilon$  is unknown.

### D. Solution of the Image Helmholtz Equation

The modal analysis to (5) gives a general solution [7]

$$U(H) = \exp(-\Lambda H)(U_{\text{Start}} - U_{\text{Final}}) + U_{\text{Final}} \quad (6)$$

where  $U_{\text{Start}}$  and  $\exp(-\Lambda H)$  are an initial image and a state transition matrix, respectively. Because of the parameter  $\varepsilon$  in (5), the state transition matrix is unknown as well. It is essentially required to determine the state transition matrix from the given domain images.

### E. Determination of the State Transition Matrix

If we have the solution  $U(H)$ , then modifying (6) yields the elements in matrix  $\Lambda$

$$\Lambda = -\frac{1}{H} \ln \left( \frac{U(H) - U_{\text{Final}}}{U_{\text{Start}} - U_{\text{Final}}} \right). \quad (7)$$

Thereby, the elements in the  $i$ th matrix  $\Lambda_i$  is determined from a series of three distinct domain images:

$$\Lambda_i = -\frac{1}{H_{i+1} - H_i} \ln \left( \frac{U_{i+1} - U_{i+2}}{U_i - U_{i+2}} \right), \quad i = 1, 2, \dots, 22. \quad (8)$$

The subscript  $i$  refers to a domain image numbered in Table I. The domain images  $U_i$  and  $U_{i+2}$  correspond to  $U_{\text{Start}}$  and  $U_{\text{Final}}$  in (6), respectively.

### F. Relation Between the Preisach Function and Matrix $\Lambda$

Since (2) and (6) are just the same expression, then the matrix  $\Lambda$  corresponds to  $(\Psi/\mu)$ . Assuming constant  $\mu$  and  $\Psi$  during  $H_i \leq H < H_{i+1}$ ,  $\Lambda_i$  obtained by means of (8) makes it possible to represent the Preisach function of its magnetization region with piecewise linear approximation.

## III. RESULTS AND DISCUSSIONS

### A. Preisach Function Distribution by Matrix $\Lambda$

Fig. 2 shows the elements in matrices  $\Lambda_i$ . The arrangement of the elements is the same as the domain pattern in Fig. 1. The elements are complex numbers due to the logarithmic function in (8). This means that the real and imaginary parts, respectively, represent in-phase and  $90^\circ$  difference phase components to the applied field. Namely, visualization of iron loss generating parts can be accomplished by the matrix  $\Lambda$ .

At first, consider the real parts of the matrices  $\Lambda$  in Fig. 2. In a small field, the moving parts of the negatively magnetized parts (black parts in Fig. 1) become zero. This means that this magnetization process is mainly carried out by the magnetic boundary displacements [left side of Fig. 2(a)] and magnetic domain movements [left side of Fig. 2(b)]. Increasing the field, the values in  $\Lambda$  represent corresponding to the rotation of magnetization [left side of Fig. 2(c)]. Because the Preisach function  $\Psi$  is the rate of change of permeability to the applied field, taking a large value in the real and imaginary parts of matrix  $\Lambda$  means that the rate of change of permeability to the applied field  $H$  is large, thereby, such a process is nonlinear in the applied field.

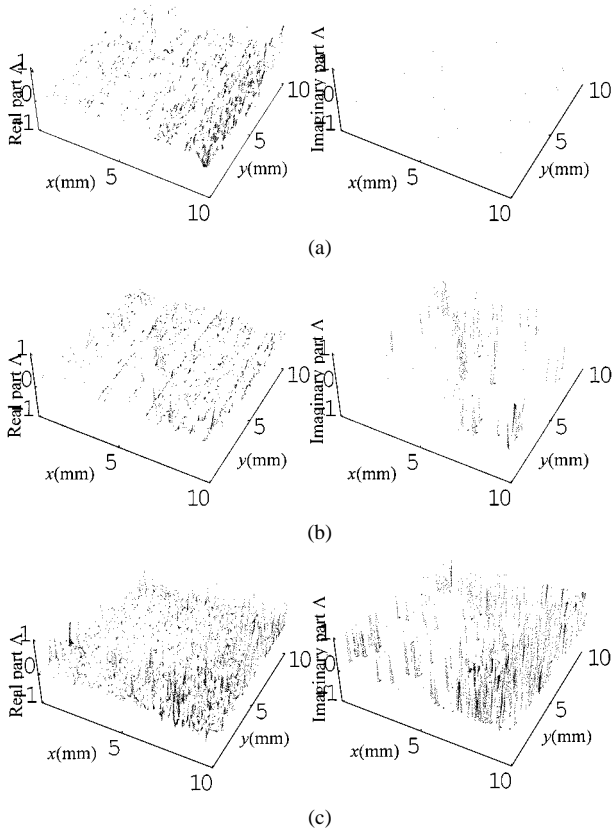


Fig. 2. Evaluated Preisach function distribution. The left and right columns are real and imaginary parts, respectively. The elements are normalized by each maximum value. (a)–(c) are constructed by the elements of matrices  $\Lambda_1$ ,  $\Lambda_2$  and  $\Lambda_9$  obtained by (8), respectively. (a)  $0.0 \leq H < 2.9$  A/m. (b)  $2.9 \leq H < 9.3$  A/m. (c)  $160.69 \leq H < 236.32$  A/m.

Conversely, a small value of  $\Lambda$  means that the rate of change of permeability to the applied field becomes small and results in linear magnetization processes.

Second, consider the imaginary parts of matrices  $\Lambda$  in Fig. 2. In a small field, the real part of this region corresponds to the magnetic boundary displacement. However, in case of imaginary part, the elements in  $\Lambda$  are close to zero [right side of Fig. 2(a)]. This means that the magnetic boundaries move without delay components. In the right side of Fig. 2(b), the values represent at the grain boundary. This is considered to be the force against the applied field. Increasing the field results in the generation of lancet domains [right side of Fig. 2(c)]. In this region, these matrix elements are then related to iron loss.

### B. Magnetization Curve

To verify our methodology, the magnetization curve is reconstructed using the evaluated Preisach function shown in Fig. 2. Substituting  $\Lambda_i$  of (8) into (6) yields domain images as the solution  $U(H)$ . Computing averaged contrast of an entire domain image gives a flux density. Fig. 3 shows the magnetization curves. Even though the domain images represent a limited area of the specimen, the experimental result supports our methodology.

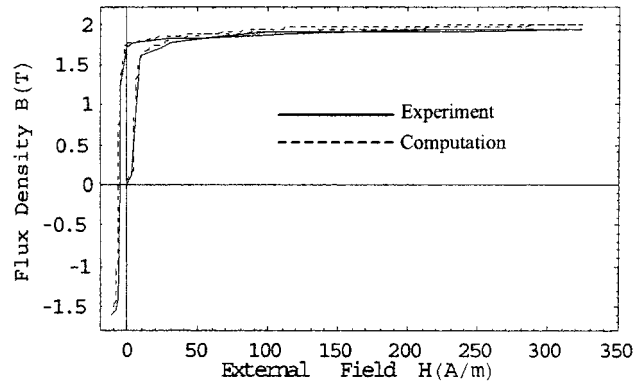


Fig. 3. Magnetization curve reconstruction based on (6).

## IV. CONCLUSION

In order to apply the Preisach model to magnetic thin-film materials, this paper has proposed an image-based approach for Preisach function calculation using a series of distinct domain images. The evaluated Preisach function is represented by the state transition matrices derived from the image Helmholtz equation. The elements of the matrices also visualize the domain dynamics such as boundary displacements, lancet domain generation, and so on. As a result of comparison with conventional measurement, we have succeeded in reproducing the magnetization curve with fairly good accuracy.

## ACKNOWLEDGMENT

The authors would like to thank Nippon Steel Corporation for providing the measurement devices, and also Dr. C. Kaido, Dr. M. Fujikura, and Dr. H. Mogi for their encouragement and helpful discussions.

## REFERENCES

- [1] F. Preisach, "Über die magnetische nachwirkung" (in German), *Zeitschrift für Physik*, vol. 94, no. 5–6, p. 277, 1935.
- [2] G. Kadar and E. D. Torre, "Hysteresis modeling: I. Noncongruency," *IEEE Trans. Magn.*, vol. MAG-23, pp. 2820–2822, Sept. 1987.
- [3] L. O. Chua and K. A. Stromsmoe, "Lumped circuit models for nonlinear inductor exhibiting hysteresis loops," *IEEE Trans. Circuit Theory*, vol. CT-17, no. 4, pp. 564–574, 1970.
- [4] A. Ivanyi, *Hysteresis Models in Electromagnetic Computation*. Budapest, Hungary: Akademiai Kiado, 1997.
- [5] S.-B. Choe and S.-C. Shin, "Magnetization reversal dynamics with sub-micron-scale coercivity variation in ferromagnetic films," *Phys. Rev. B*, vol. 62, no. 13, pp. 8646–8649, 2000.
- [6] A. Hubert and R. Schäfer, *Magnetic Domains*. Berlin, Germany: Springer-Verlag, 2000.
- [7] H. Endo, S. Hayano, Y. Saito, and T. L. Kunii, "A method of image processing and its application to magnetodynamic fields" (in Japanese), *Trans. IEE Japan*, vol. 120-A, no. 10, pp. 913–918, 2000.
- [8] Y. Saito, S. Hayano, and Y. Sakaki, "A parameter representing eddy current loss of soft magnetic materials and its constitutive equation," *J. Appl. Phys.*, vol. 64, no. 1, pp. 5684–5686, 1988.
- [9] T. Nozawa, T. Yamamoto, Y. Matsuo, and Y. Ohya, "Effects of scratching on losses in 3-percent Si-Fe single crystals with orientation near (110) [001]," *IEEE Trans. Magn.*, vol. 15, pp. 972–981, Mar. 1979.
- [10] H. Endo, S. Hayano, Y. Saito, and T. L. Kunii, "Image governing equations and its application to vector fields" (in Japanese), *Trans. IEE Japan*, vol. 120-A, no. 12, pp. 1089–1094, 2000.